Arabian Journal of Geosciences (2022) 15: 483
https://doi.org/10.1007/s12517-022-09691-2

ORIGINAL PAPER

Experimental and numerical examination of flow resistance in plane bed streams

Vahid Hassanzadeh Vayghan[1] · Mirali Mohammadi[1] · Behzad Shakouri[1]

Received: 4 October 2021 / Accepted: 10 February 2022 / Published online: 8 March 2022

Abstract

Water flow in a plane bed stream (PBS) is different from the conventional open channels because of a higher ratio of "width to depth, (*b/h*)". Although much research has been carried out on the hydraulics of flow in PBSs, but the flow characteristics have not been fully understood yet. Thus, understanding flow resistance is necessary for flood prediction and flood routing. In the present research work, a comprehensive examination of hydraulics characteristics of PBSs is conducted by using both physical and Flow-3D numerical models of a wide rectangular channel with various sizes of bed materials. A stage-discharge relationship was developed for a PBS using four different types of bed materials. Results of the physical model indicated that for the discharges higher than 0.035 m^3/s, by increasing the bed roughness, the Manning's roughness, *n*, increased within 3%. Results of the numerical model showed that by increasing the Froude number, *Fr*, Manning's roughness, *n*, decreased linearly. Finally, a novel general linear equation for calculating Manning's roughness coefficient, *n*, including all related parameters, was also obtained that can be used by the hydraulic engineers and institutional river managers.

Keywords Plane stream · Physical model · Stage-discharge · Flow velocity · Manning's roughness · FLOW-3D

Introduction and literature survey

The economy and effectiveness of many water resources projects are related to the determination of flow resistance in channels (Kumar and Bhatla 2010). The difficulty of flow resistance determination is because the flow boundary in alluvial channels is not fixed but its characteristic geometry and dimensions through mutual interaction between the flow and bed continuously are changing (Kumar 2011). Flow resistance affects the velocity and hence flow depth, and also, it controls the distribution of shear stress around the channel boundary and, therefore, the magnitude and distribution of bed and bank erosion. Thus, it is an absolute control of flow hydraulics in streams and rivers, so a thorough understanding of flow resistance is necessary for flood prediction and flood routing and many geomorphological, sedimentological, and engineering studies and design of channel form, stability and adjustment, ecological habitat prediction, sediment routing models, and other scientific and practical applications (Ferguson 2007; 2010; 2012; Nitsche et al. 2011; Powell 2014; Hou et al. 2019; Iraji et al. 2020; Satvati et al. 2020; Zheng et al. 2021).

Flow resistance in open channels can stem from four different factors: (1) surface or skin friction, (2) form resistance or drag, (3) wave resistance from free surface distortion, and (4) resistance associated with local acceleration or flow unsteadiness (Rouse 1965; Yen 2002). The Manning's roughness coefficient, *n,* can be derived using the well-known Darcy-Weisbach equation, in the form of $n \Big/ k_s^{1/6}$ (Yen 2002). Leopold et al. (1964) divided the resistance into those due to skin friction, internal distortion, and spills (Yen 2002). The Moody diagram is a particular form of the Darcy-Weisbach equation (Rouse 1965). Flow resistance generally depends on the distribution of velocity. According to the boundary layer theory, the distribution of velocity *u* along the wall-normal *y*-direction is adequately described by two universal laws; namely, the inner law or law of the wall

Responsible Editor: Broder J. Merkel

✉ Mirali Mohammadi
m.mohammadi@urmia.ac.ir

Vahid Hassanzadeh Vayghan
v.hasanzadeh@urmia.ac.ir

Behzad Shakouri
b.shakouri@urmia.ac.ir

[1] Department of Civil Engineering, Faculty of Engineering, Urmia University, P O Box 165, 57561-15311 Urmia, Iran

where the viscous effect dominates, and the outer law or velocity defect law)Rouse 1965; Hinze 1975; Schlichting and Kestin 1961; Yen 2002). The flow regions of the inner and outer law are not entirely separate, and there is an overlapping area between them. The logarithmic function of well-known Darcy-Weisbach can be applied for the velocity distribution in both regions as Eq. 1 (Yen 2002):

$$\frac{u}{u_*} = C_1 \log y^* + C_2 \tag{1}$$

where C_1 and C_2 are constant and u_* is shear velocity. Based on Yen (2002), the resistance due to steady uniform flow can only be a function of the Reynolds number and relative roughness, and the effect of the Froude number may be ignored (as Eq. 2):

$$f, \frac{n}{R^{1/6}}, \frac{C}{\sqrt{g}} = F\left(Re, \frac{k_s}{R}\right) \tag{2}$$

Equation 2 is also based on the Moody diagram. Equations of Manning, Chezy, and Darcy-Weisbach (Eq. 3), are also widely used to calculate the velocity using the flow resistance coefficient (Yen 1991, 2002):

$$U = C\sqrt{RS_0} = \sqrt{\frac{8g}{f}}\sqrt{RS_0} = \frac{K_n}{n}R^{2/3}S_0^{1/2} \tag{3}$$

where C, f, and n are the Chezy, Weisbach, and Manning roughness coefficients, respectively; R is hydraulic radius; S_0 is slope; g is gravitational acceleration; and K_n is 1 $m^{1/2}/s$ for U and R in SI units, 1.486 $ft^{1/3}$-$m^{1/6}/s$ for English units, and $\sqrt{g}$ dimensionally homogeneous Manning formula (Yen 2002). Yen (1992) proposed a general expression to represent the overall resistance of composite channels (Eq. 4)

$$n_c = \sum_{i=1}^{m} w_i n_i \tag{4}$$

where m is the number of sub-cross-sections of a combination of area A_i, wetted perimeter P_i, or the hydraulic radius R_i; w_i is the ith weighting function, and n_i is the ith local Manning n value. There are over ten equations based on the concept of Eq. 4 that have been proposed (see Mohammadi 1998 for more detail). In this research, Lotter (1933) equations were used for determining different roughness of the bottom and walls of the model (Eq. 5)

$$n_c = \frac{PR^{\frac{5}{3}}}{\sum \frac{PR^{\frac{5}{3}}}{n_i}} \tag{5}$$

To detect the flow regime (hydraulically smooth, transitional, and rough turbulent flow), the shear Reynolds number, Re_*, is used, as given in Eq. 6 (Powell 2014).

$$Re_* = \frac{u_* k_s}{\nu} \tag{6}$$

where k_s is the thickness of the roughness. To calculate u_*, the logarithmic profile of velocity was drawn at each section, and the slope of the velocity profile was also calculated. Then, by inserting it on a related general equation, the shear velocity was obtained as Eq. 7 (Nezu and Rodi 1986).

$$u_* = \frac{M.\kappa}{2.303} \tag{7}$$

where M is the slope of the logarithmic profile of the cross-sectional velocity and κ is the von-Kármán universal constant that equals to 0.40–0.41, which is widely used to describe the grain resistance of a plane bed on the assumption that the velocity profile is logarithmic (Nezu and Rodi 1986; Ferguson 2012). Typically, smooth turbulent flow, transitional flow, and rough turbulent flow are defined by $Re_* \leq 3.5$, $3.5 \leq Re_* \leq 68$, and $Re_* \geq 68$, respectively (Powell 2014).

To determine the type of rivers, the characteristics of the geometric shape of the river sections, which include meandering, shape, *b/h* aspect ratio, and degradation rate, are used (Buffington and Montgomery 1999; 2013). According to the Rosgen classification, rivers located in the B type are mainly wide rivers with plane beds. Wide rivers with plane beds have low flow depths and high *b/h* aspect ratios and occur in the middle and end sections of the longitudinal section of rivers (Rosgen 1994; 2003; Rosgen and Silvey 1996). Some of the recent researches on river type classifications are conducted by Kasprak et al. 2016; Horacio et al. 2017; 2018 and else.

Myers (1982) calculated the friction coefficients for the rectangular channels with *b/h* (aspect ratio) of 1 to 35 and examined *b/h* effects on friction coefficients. Then, Myers (1982) reported a low correlation between *b/h* and friction coefficient, likely due to the presence of secondary flows and non-uniform shear patterns. Dolgopolova (2001) vastly studied the flow resistance in the plane rivers using the Darcy-Weisbach friction factor, *f*. By providing the cross-sectional shape coefficient, *m*, Dolgopolova (2001) obtained a theoretical value for plane rivers to be equal to 2 and compared it with the results of field studies related to some Russian rivers. The results obtained by Dolgopolova confirmed the use of coefficient $m = 2$ for wide-plane channels. For the flows with $h/b \ll 1$ (i.e. $b/h \gg 1$), Dolgopolova (2000) used $f = 0.32n^2$ and calculated the coefficient of friction in several plane rivers. The results of Dolgopolova indicated that in the rivers considered, where the aspect ratio, *b/h*, is above 33, and therefore, $m = 2$ can be applied.

Starting from a plane bed without sediment transport, ripples, dunes, and washed-out dunes develop in large experimental flumes as the flow intensity increases in magnitude

over a bed of loose sand particles (see Julien 2010 and Roushangar et al. 2017; for more detail). Many classic friction factor models have been developed, which describe the complex phenomenon of flow resistance. Meyer-Peter and Müller (1948), Einstein and Barbarossa (1952), Taylor Jr and Brooks (1962), Raudkivi (1967), Richardson and Simons (1967), Smith (1968), Van Rijn (1984), Karim (1999), Yang et al. (2005), and van der Mark et al. (2008) have all presented expressions for the total friction factor resulting from bedform roughness (Roushangar et al. 2017). Mohammadi (2002) investigated the effect of secondary flows and cross-sectional shape on the distribution of boundary shear stress and flow resistance coefficients, by performing various experimental sets on V-shaped bottom channel cross-section with vertical walls. Mohammadi (2002) attempted to develop a relationship for determining the flow resistance in rectangular and circular channels' cross-sections. Javid and Mohammadi (2012) focused on the hydraulic radius separation approach used to calculate the flow resistance and boundary shear stress in terms of bed and wall shear stress proposed in a trapezoidal channel.

Continuous flow measurement in rivers and channels, even in normal conditions, is costly and complicated, so we need to develop general equations to estimate the water discharge based on easily-measurable flow parameters. A stage-discharge relationship is a resistance-to-flow relationship (White et al. 2005). Several investigators have proposed accurate approaches for this purpose. Sefe (1996) conducted a study to provide the stage-discharge relationship of the Okavaiigo River at Mohembo, Botswana. Sterling and Knight (2000) investigated the stage-discharge curve in circular conducted with and without a plane bed. Based on field measurement results, Cantalice et al. (2013) proposed a stage-discharge relationship to estimate the discharge in Exu River, Brazil, with sand bed materials of $d_{50}=0.77$ mm. Parsaie et al. (2017) presented some relations to estimate the flow discharge in a different compound channel roughness. Results all indicated that the effect of different roughness on the stage-discharge relation at low values of discharge is visible, whereas increasing the value of discharge is decreased. Some of other researches in the concept of stage-discharge are such as Léonard et al. (2000); Jain and Chalisgaonkar (2000); Abril and Knight (2004); Sivapragasam and Muttil (2005); Maghrebi (2006); Rahimpour and Maghrebi (2006); Guven and Aytek (2009); Yang et al. (2014); Singh et al. (2014); Hasanpour Kashani et al. (2015); and Maghrebi et al. (2016).

Due to a higher aspect ratio, b/h, in PBSs, hydraulic features in those streams are different from the conventional open channels. Thus, hydraulic characteristics in PBSs, including flow patterns, stage-discharge relationship, velocity distribution, flow resistance, and shear stress, need to be separately investigated using laboratory and numerical modeling techniques. This research work for the first time conducts a comprehensive study on hydraulic characteristics of PBS models, including the flow resistance and stage-discharge relationships as well as velocity and shear stress. Also, experimental equations for obtaining Manning's roughness coefficient, n, are presented using the results of the hydraulics and numerical models. The advantages of this model compared with the other researches are: (1) reducing the scale effects due to building a vast and extended model, (2) creating a higher ratio of b/h as aspect ratio and reviewing the relevant results, (3) development of the results for plane streams with different bed slopes using a numerical simulation. Results of the present study can be used to investigate and identify the hydraulic characteristics of wide and plane bed rivers. Based on those characteristics, hydraulic engineers can design intersecting structures. Also, institutional river management, necessary flood forecast, and sediment management can be conducted.

Methodology

In this research, by using a physical model of a wide rectangular channel (as described in the "Physical model" section), and various sizes of bed material and then by developing the FLOW-3D software model, hydraulic characteristics of PBS are investigated. To this aim, four different bed materials, including concrete, sand, fine gravel, and coarse gravel, are used to evaluate the effects of roughness on flow resistance. Also, three different channel bed slopes are used to study the effect of bed slope changes on the hydraulic parameters of the plane stream models. Figure 1 shows the flowchart of the total steps used in the present study.

Dimensional analysis of the Manning's roughness coefficient, *n*

The essential parameters in determining the Manning roughness coefficient, n in the channels are as a function of Eq. 8.

$$n = f\left(U, h, b, \rho, g, \mu, k_s, S_o\right) \tag{8}$$

where U is mean velocity, h is flow depth, μ is the viscosity of water, ρ is water density, g is gravity acceleration, k_s is the average particle size of bed material, and S_o is the channel bed slope. Considering h, U, and ρ are repetitive variables, the Manning's roughness coefficient, n, could be described by the Buckingham Pi analysis approach, as given by Eq. 9:

$$n = f\left(Re, Fr, S_0, \frac{b}{h}, \frac{R_h}{k_s}\right) \tag{9}$$

Herein, the b/h aspect ratios and R_h/k_s are dimensionless numbers that are widely used in surveying the hydraulics

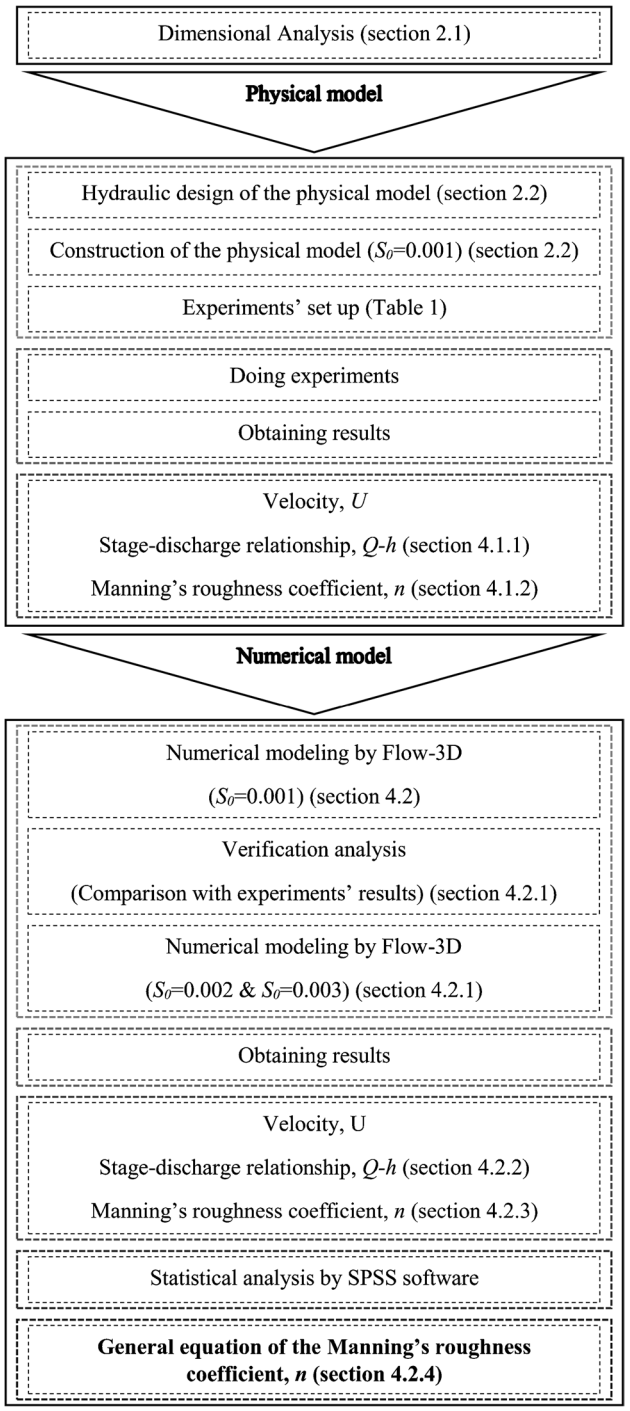

Fig. 1 Flowchart of the total steps used in the present study

aspects of rivers and channels, S_0 is the channel bed slope, and it was 0.001 in the present physical model. For developing this research, using the well-known FLOW-3D software, two more channel bed slopes of 0.002 and 0.003 were also modeled and evaluated. Therefore, the term of channel bed slope (S_0) was also investigated.

Physical model

A model of PBS, with a concrete bed, a rectangular cross-Sect. (1.5 m width and 0.45 m height), 60 m length, and longitudinal bed slope of 0.001 was constructed and used for the first step of the experiments that contained several measurements tabulated in Table 1. To investigate the effects of different bed materials, a section with a length of 13 m and a thickness of 0.1 m (10 cm deeper than the bed level) was designed in the middle of the channel. In the next steps of experiments, 10 cm extra depth in this section was filled with different materials (i.e., sand and gravel) and used for bed roughness experiments (see Figs. 2 and 3 in detail).

The Plane Bed Stream Physical Model (PBSPM) consisted of the following: (1) upstream reservoir, (2) stilling basin, (3) entire laboratory measuring channel, (4) discharge measuring basin, (5) downstream reservoir, (6) pump, (7) pipe system for water transfer to upstream, and (8) the "location of bed material's change (LBMC)" which are graphically shown in Fig. 2.

To adjust the flow depth in the model and develop a steady flow in the measurement section, a steel tailgate with 1.5 m width and 0.4 m height was used (Fig. 2). The discharge measuring basin was constructed with 1.9 m × 1.85 m dimensions with a depth of 1 m, and a rectangular sharp crest weir was installed at the end of the basin (Fig. 2). To prevent the loss of water, the insulation of the model components was carried out using a thick plastic sheet. A pumping system was developed to create a flow circulation in the model and transfer water from the pool downstream to the reservoir upstream. The pump used in the model was a 150–200 centrifuge pump manufactured by Pumpiran Company, Tabriz, with a maximum discharge of 0.1 m^3/s. The pump was coupled with a 15-KW electromotor and mounted on the respective chassis (Fig. 2), which used a 200 mm diameter polyethylene pipe with a length of 68 m for the pump discharge pipe. Flow rates of 0.005 to 0.075 m^3/s were considered and flowed in the physical model by 0.005 m^3/s increments. In the first step of the experiments, four different depths were created by tailgate for each flow discharge to determine the standard depth and stage-discharge relationship in the channel with a concrete bed. The surface profile was taken for each experiment with different depths using a pointer gauge. The measurements were carried out in left, right, and middle lines at 2 m intervals along the channel. After performing the experiments on a concrete bed, the bed materials of the model were replaced by sand, fine-grained and coarse gravel in the "LBMC" to evaluate the hydraulic performance of PBSPMs. Table 1 designates the measured parameters and the number of experiments.

The flow profile in the "LBMC" was measured using a wheeled point gauge with a precision of ± 0.1 mm (by Adak Iranian Co., Tabriz). The measurements were carried out

Table 1 Measured parameters and the number of experiments in the PBSPM

Bed material	Measured parameters	No. of experiments	Sum
Concrete	Tailgate	60	105
	Stage-discharge	15	
	Longitudinal and cross-sectional profile (flow depths)	15	
	Velocity	15	
Sand	Stage-discharge	15	45
	Longitudinal and cross-sectional profile (flow depths)	15	
	Velocity	15	
Fine gravel	Stage-discharge	15	45
	Longitudinal and cross-sectional profile (flow depths)	15	
	Velocity	15	
Coarse gravel	Stage-discharge	15	45
	Longitudinal and cross-sectional profile (flow depths)	15	
	Velocity	15	

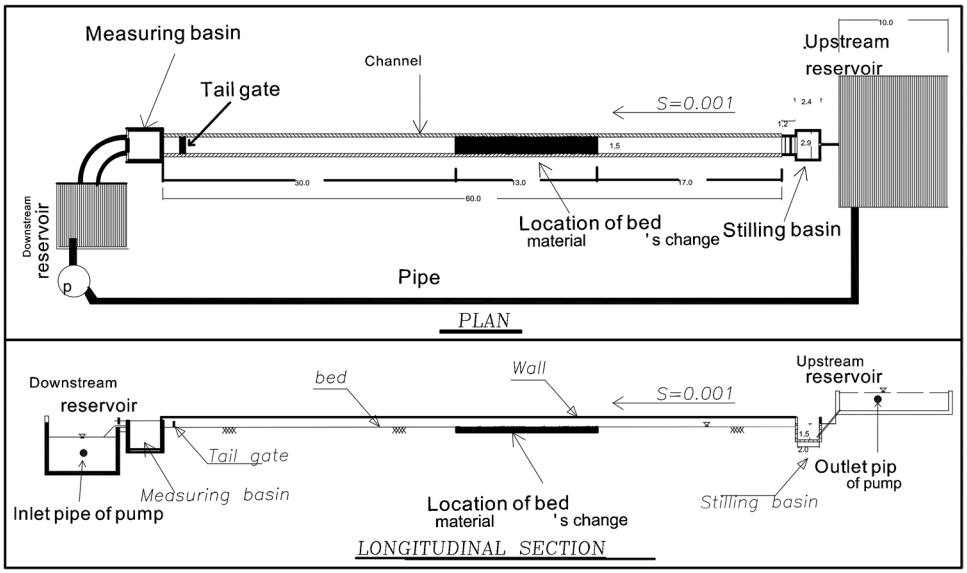

Fig. 2 A plan view and longitudinal section of the physical model (dimensions in meters)

in left, right, and middle lines at 2 m intervals along with the "LBMC" (in 5 points). The discharge of outgoing flow from the channel was measured using a stilling basin and a calibrated rectangular weir at the end of the basin. The water level on the crest of the rectangular weir was measured by a pointer gauge with a precision of ± 0.1 mm. To measure the flow velocity in the channel, the current meter (micro flowmeter) from Armfield UK was used.

The determination of material sizes used on the channel bed was carried out in the geotechnical laboratory. Based on the material granulation curve (MGC), the mean grain size (d_{50}) for sand, gravel, and coarse gravel is 2, 10, and 20 mm, respectively. After testing on a concrete bed, as for the first step of experiments, the surface concrete of the "LBMC" was destroyed, sands were deposited in the site, and a bed slope of 0.001 was created. The next step of the experiments was to change the bed materials for land grading and preparation of the bed materials (Fig. 3a–c).

Based on the flow profiles obtained from the experiments conducted on the concrete bed, the diagrams for the flow slope-depth were plotted versus the tailgate indicator for different discharges, and the uniform flow depth was obtained. The stage-discharge-tailgate diagram for the model was then produced. By adjusting the tailgate by the stage-discharge-tailgate curve, in all experiments, an average depth was created. Then, measurements of the surface flow profile at the "LBMC" were made for four different types of bed material as explained before. Due to the average velocity and standard depth measured for the PBSPM, the hydraulic radius was calculated, and the shear velocity was calculated by substituting in Eq. 7. Reynolds shear number was calculated by considering $k_s = 3$ mm for concrete bed (Akan

(a) (b) (c)

Fig. 3 Channel bed preparation of the bed materials: **a** sand bed, **b** fine gravel bed, **c** coarse gravel bed

2006), $k_s = 5$ mm for sandy bed (Lopez and Barragan 2008), and $k_s = 7$ mm for fine gravel bed and $k_s = 10$ mm for coarse gravel bed (Yang 1996).

FLOW-3D numerical model

The FLOW-3D software is suitable for the simulation of shallow water flow, viscosity, cavitation, and turbulent flow. The governing equations in this model are the well-known Navier–Stokes equations together with the continuity equation. FLOW-3D solves the Navier–Stokes equations using the Finite Volume Method (FVM) on a displaced network. Then, the volume of fluid (VOF) method is usually used for the free surface simulation (see Flow Science Inc. 2008 for more information).

The process of implementing FLOW-3D

The 3D geometric range of flow was determined based on the dimensions of the physical model and hydraulics characteristics of flow. The geometric range consists of three surfaces (two walls and one bed). In this research work, the network range was 60 m in length, with an internal width of 1.5 m and a depth of 0.45 m. According to the bed slope of the channel model, using the related tool, the geometry of the model was rotated around the y-axis. After defining the desired range, gridding was carried out in the 18 m range in the station of 17 to 35 m of the channel. The number of network elements in the computing range was 13,000.

Definition of boundary conditions

The final stage in networking is defining the boundary conditions. In the FLOW-3D model, the boundary conditions are defined for the minimum and maximum values of x, y, and z for the geometric model.In this study, the boundary conditions are given in Table 2.

The roughness of the bed, proportional to the intended materials for the physical model, was changed in the models. In FLOW-3D, the thickness of bed roughness for simulation of the concrete is $k_s = 3$ mm, for the sand bed is $k_s = 5$ mm, for the fine gravel bed material $k_s = 7$ mm and for the coarse gravel bed material $k_s = 10$ mm were considered. The free surface flow option was selected in the general specifications as well as the hydraulic data options in the output section of the model. The flow analysis was performed in the case of steady flow, and the Re-Normalization Group (RNG) k-ε turbulence model was used. Target flow rates were as follows: 0.1, 0.2, 0.3, 0.4, 0.5, 0.6, and 0.7 m^3/s for all models with different bed materials and different bed slopes. Eventually, the results of the FLOW-3D model were compared with the physical model. The statistical equation (Eq. 10) has been used to determine the average relative error between the calculated values by the software and the values of the physical model.

$$\%E = \frac{\left|c_m - c_p\right|}{c_m} \times 100 \tag{10}$$

where $\%E$ is percentage error, c_m is the hydraulic parameter value measured in the physical model, and c_p is the hydraulic parameter value estimated by the FLOW-3D model.

Results and discussion

Physical model

Stage-discharge relationships

Measurements of the surface flow profile at the "LBMC" were made for four different types of bed material. In Fig. 4a, a comparison of the normal flow depth at discharges 0.4 and 0.7 m^3/s is provided for four different bed materials. Figure 4a shows that by increasing bed roughness, the flow depth increases with the same proportion in all bed materials. Also, due to passing the flow from smooth concrete bed to the rough bed in the "LBMC," the longitudinal profile of the flow had a gradual increase at the distance of 17 m

Table 2 Boundary conditions in the Plane Bed Stream Numerical Model (PBSNM)

X min	*X max*	*Y min*	*Y max*	*Z min*	*Z max*
Flow inlet	Flow outlet	*Wall*	*Wall*	*Bed*	*Atmosphere*
Volume of flow	*Outflow*	*Wall*	*Wall*	*Wall*	*Symmetry*

(i.e. beginning of the "LBMC") and at the end of "LBMC," longitudinal profile reaches to normal depth. Concerning depth in the middle of the "LBMC" as a normal depth, the stage-discharge equation was calculated for the PBSPM with four different bed materials and compared with the stage-discharge curve of the concrete bed (Fig. 4b). Based on Fig. 4b, the stage-discharge relationship for different bed materials is according to Table 3.

According to Fig. 4b and Table 3, it is shown that by increasing bed roughness, the coefficient of relationships and the exponent of stage-discharge relationship increase by 3% and 1.5%, respectively. This means that the flow resistance caused by the roughness of bed materials increases the flow depth in a constant flow discharge. The results for the stage-discharge of sand bed model have a higher coefficient than that of the Exu river (with $d_{50}=0.77$ mm) stage-discharge relationship (Cantalice et al. 2013) because the physical model bed is relatively smoother than the natural river bed (which causes a flow with a lower depth in a constant discharge). Based on the results obtained for the flow depth, it was found that the *b/h* aspect ratio in all discharges is greater than 12, and therefore, according to Rosgen classification (Rosgen 2003), these flows are considered plane rivers. To control the instability of the flow, the shear Reynolds number, and to study the flow regime during the experiments, two non-dimensional numbers of Froude and Reynolds were calculated, and their graphs were plotted versus the flow depth (Fig. 5).

Considering Fig. 5a, it is found that the obtained Re_* number is greater than 70 and the flow is in a turbulent regime in all flow discharges. As the bed roughness increased, the shear Reynolds number increased as a result of the development of boundary layer and turbulence due to the flow. Concerning Fig. 5b–c, it was found that for all discharges of the model, the flow regime was subcritical-turbulent.

Analysis of Manning's roughness coefficient, n

Based on the measured velocity, flow depth, and discharge, the Manning's roughness coefficient, *n*, is calculated using the Manning formula (Fig. 6). According to Fig. 6a, it can be stated that as the flow discharge increased, the Manning's roughness coefficient, *n*, due to the flow decreased. This trend is quite evident in coarse gravel materials with a discharge of less than 0.035 m^3/s, but in the sand and fine gravel beds, the trend is reduced. Generally, in a discharge greater than 0.035 m^3/s, by changing the bed materials from sand to fine gravel and coarse gravel, Manning's roughness coefficient increased about 3%. According to Fig. 6b, it can be stated that by increasing the flow depth (*h*), the flow roughness decreased. The reduction trend for *n* values in a coarse gravel bed is higher than sand and fine gravel bed materials.

To determine the effect of Froude and Reynolds numbers, the ratio of the hydraulic radius to the roughness thickness (R_h/k_s), and *b/h* aspect ratio on the Manning's roughness coefficient, *n*, the measured *n* values plotted (see Fig. 7a–b). Regarding Fig. 7a–b, it is shown that by increasing *Fr* and *Re* numbers, the Manning's roughness coefficient, *n*, decreases for all models. The gradient of those changes in coarse gravel material is high compared with two other materials of sand and fine gravel materials. This is due to the higher turbulence intensity in rougher beds. Figure 7c shows that by increasing R_h/k_s, Manning's *n* is decreased. The overall equation of the R_h/k_s ratio and *n* in a bed slope, $S_0=0.001$, is presented in Eq. 15.

$$n = 0.022 - 0.0003\left(\frac{R_h}{k_s}\right) \tag{15}$$

In the present work, the *b/h* aspect ratio is the primary independent variable, so discharge changes are reflected. To establish a general equation for the Manning's roughness coefficient, *n*, in terms of different *b/h* aspect ratios, the graphs of *n* versus *b/h* were drawn for all models (Fig. 7d). Equations for the Manning's roughness coefficient, *n*, and *b/h* aspect ratio for each bed material are given in Table 4 used depending upon the types of the PBSs.

According to Fig. 7d and Table 4, it is shown that by increasing the *b/h* aspect ratio, the Manning's roughness coefficient, *n*, increases. In all bed materials, the slope of *n* increases sharply for *b/h* aspect ratios that are less than 20, but at higher *b/h* aspect ratios (more than 20), this slope is a bit milder. This is due to the effect of the expansion of the flow boundary layer in terms of flow depth. Also, by increasing bed roughness, the effect of the *b/h* aspect ratio on the *n* values increases (especially in wide river flows).

Numerical model

After implementation of numerical models, hydraulic parameters of flow including flow depth, velocity, and *Fr* number were stored graphically and textually, and used

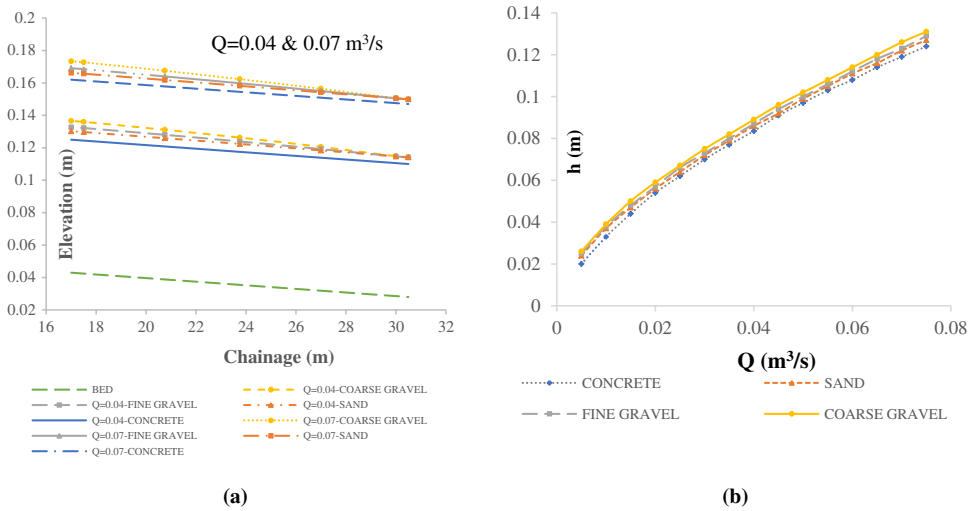

(a) (b)

Fig. 4 **a** Flow profiles in PBSPM for flow in different bed materials. **b** Stage-discharge curve for PBSPM

in the analysis of the model. As an example, flow depth contours in a cross-section by Flow-3D with a bed slope of 0.001 and a discharge of 0.7 m^3/s for different bed materials are presented in Fig. 8a–d.

Verification of numerical model

For verifying the results of the numerical model, the flow rate of 0.1 to 0.7 m^3/s was applied in the model with a bed slope of 0.001, and graphical and textual results were obtained. The results of the numerical model were compared with the results of the physical model, and the percentage error was calculated. In Fig. 9, the results of stage-discharge and average flow velocity in various bed materials in both numerical and physical models are compared. The percentage error of depth and averaged flow velocity are presented in Table 5. The errors were derived via Eq. 10.

According to Fig. 9 and Table 5, it is determined that the FLOW-3D model gives acceptable agreements for estimating the flow depth (within 2.25%) and flow velocity (less than 4%) in a PBS. Therefore, it can be stated that the FLOW-3D model has sufficient accuracy to develop research on a PBS model with bed slopes of 0.002 and 0.003. After verifying the results, a numerical model was simulated for all discharges and bed materials at two bed slopes of 0.002 and 0.003.

Table 3 Stage-discharge relationships for PBSPM ($S_0 = 0.001$) (Eqs. 11–14)

Bed material	*Stage-discharge relationships (Q (m^3/s) and h (m))*	*Equation no*	R^2
Concrete	$Q = 1.654 \times h^{1.497}$	*Equation 11*	*0.9992*
Sand	$Q = 2.155 \times h^{1.626}$	*Equation 12*	*0.9995*
Fine gravel	$Q = 2.238 \times h^{1.652}$	*Equation 13*	*0.9994*
Coarse gravel	$Q = 2.275 \times h^{1.673}$	*Equation 14*	*0.9992*

Stage-discharge relationships

Stage-discharge curves for the model with above bed slopes are shown plotted in Fig. 10.

It can be seen from Fig. 10a that for $S_0 = 0.002$ at discharges of less than 0.3 m^3/s, the trend of the stage-discharge curve is sharper than discharges greater than 0.3 m^3/s. According to Fig. 10b, it is determined that the stage-discharge curves are likely linear. In Fig. 10a–b, the flow depth increases by increasing bed roughness. The stage-discharge relationships for each bed material in both mentioned slopes are given in Table 6.

In the case of the bed slope of 0.002 for the concrete, sand, and fine gravel bed, the power and the coefficient of the stage-discharge relationships decrease by increasing the bed roughness, but this trend changes in the case of coarse gravel material. On the bed slope of 0.003, the coefficient of the stage-discharge relationship decreases by increasing the roughness of the bed, but the power of the relationship increases by increasing bed roughness. A comparison of these relationships with the results given by the physical model shows that the coefficient of the relationship increases from 10 to 20%, and the power of the relationship increase from 5 to 10% from concrete to coarse gravel bed materials.

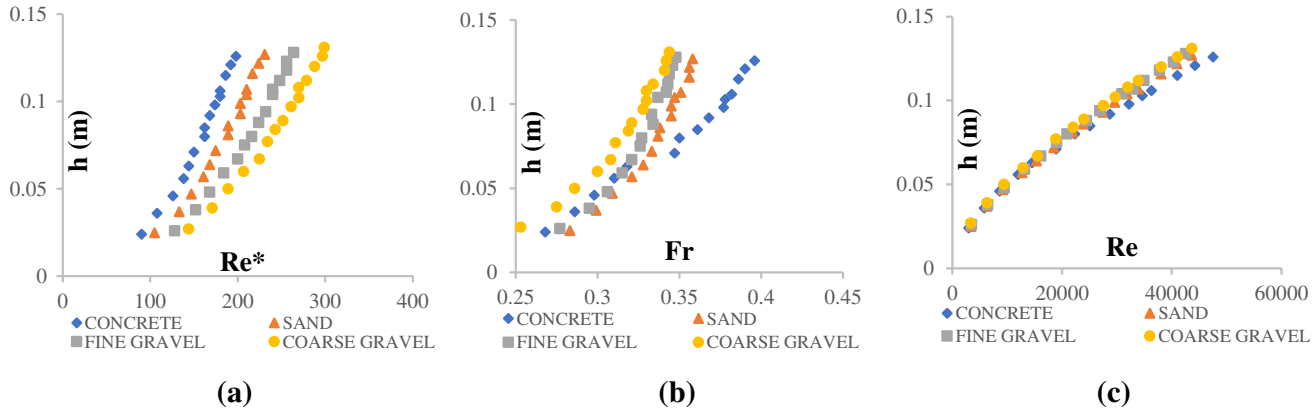

Fig. 5 Variations in **a** shear Reynolds (*Re**), **b** Froude (*Fr*), and **c** Reynolds (*Re*) numbers versus flow depth (h) in PBSPM

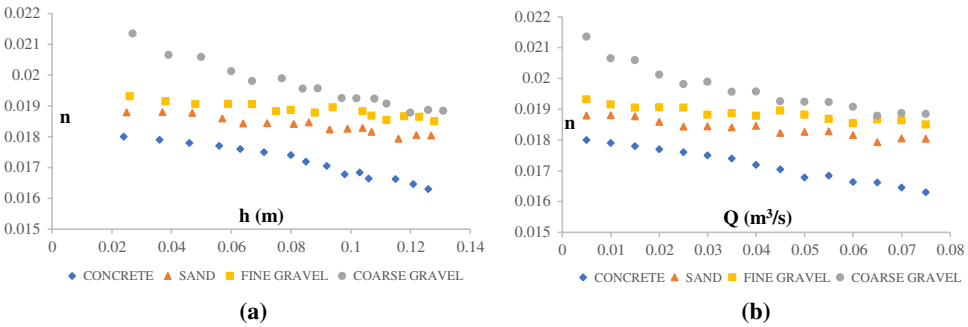

Fig. 6 Variations of measured *n*, versus **a** flow depth, *h* and **b** discharge, *Q*

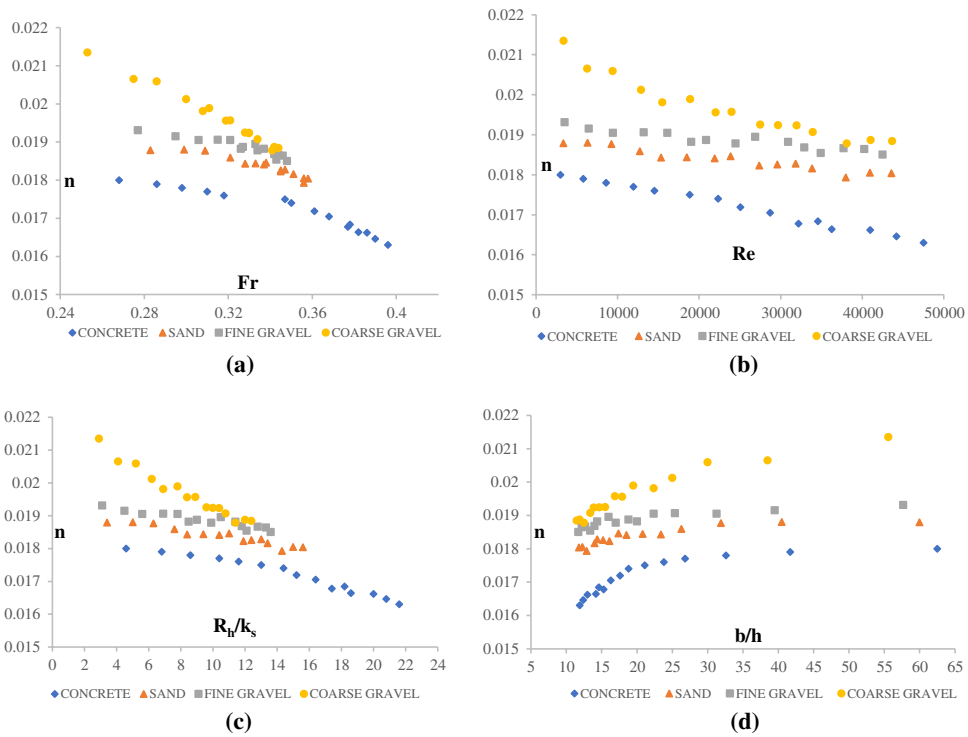

Fig. 7 Variations of measured *n* versus **a** *Fr* number, **b** *Re* number, **c** R_h/k_s, and **d** *b/h*

Table 4 Equations for the Manning's roughness coefficient, *n*, and *b/h* aspect ratio in PBSPM (Eqs. 16–19)

Bed material	*Equation*	*Equation no*
Concrete	$n = 0.00846 + 0.00073\left(\frac{b}{h}\right)$	Equation 16
Sand	$n = 0.0174 + 0.00006\left(\frac{b}{h}\right)$	Equation 17
Fine gravel	$n = 0.0182 + 0.00004\left(\frac{b}{h}\right)$	Equation 18
Coarse gravel	$n = 0.0175 + 0.0001\left(\frac{b}{h}\right)$	Equation 19

The Manning's roughness coefficient, *n*

Figure 11 shows the variations of Manning's roughness, *n*, versus *Fr* and *Re* numbers in models with bed slopes of 0.002 and 0.003.

Concerning Fig. 11, it is evident that by increasing the *Fr* number, Manning's roughness coefficient, *n*, decreases on both slopes. The change range of *n* is between 0.013 and 0.027, and the *Fr* number in both models with slopes of 0.002 and 0.003 was between 0.15 and 0.49. A comparison of the results for the two models shows that the relationship trend in the model of $S_0 = 0.002$ is sharper than that of $S_0 = 0.003$. According to Fig. 11, by increasing *Re* number, on both bed slopes, the Manning's roughness coefficient, *n*, decreases between 0.027 and 0.013. Diagrams of Manning's roughness coefficient, *n*, versus the ratio of "hydraulic radius to the thickness of bed roughness, (R_h/k_s)" and *b/h* aspect ratio are presented in Fig. 12.

It can be seen from Fig. 12 that Manning's roughness coefficient, *n*, decreases by increasing the ratio of R_h/k_s. Equations between *n* and R_h/k_s are presented in Table 7.

According to Table 7, it is evident that for the same values of R_h/k_s in the above equations, the Manning's roughness coefficient, *n*, obtained from the equation of $S_0 = 0.002$ is higher than that of $S_0 = 0.003$. From Fig. 12, it is also seen that by increasing *the b/h* aspect ratio in all bed materials, roughness coefficient, *n*, increases, and by increasing the R_h/k_s, the effect of *b/h* aspect ratio on the Manning's roughness coefficient, *n*, increases.

General equation of the Manning's roughness coefficient, *n*

To determine a general equation for calculating Manning's roughness coefficient, *n*, using the SPSS statistical software and the linear regression method, the determined independent parameters in the dimensional analysis were entered into the software and the overall equation was obtained as Eq. 32. The specification of the model and R^2 of the equation is given in Table 8.

$$n = 0.036 - 0.42Fr - 0.486S_0 - 0.000044\left(\frac{b}{h}\right) - 0.000068\left(\frac{R}{k_s}\right) \quad (32)$$

By examining the results (according to Table 8), it is determined that the general Eq. 32 calculated the values of Manning's roughness coefficient, *n*, very well, and gives a low percentage error (3.15%), so Eq. 32 can be used by the hydraulic engineers and institutional river managers for plane bed rivers and streams.

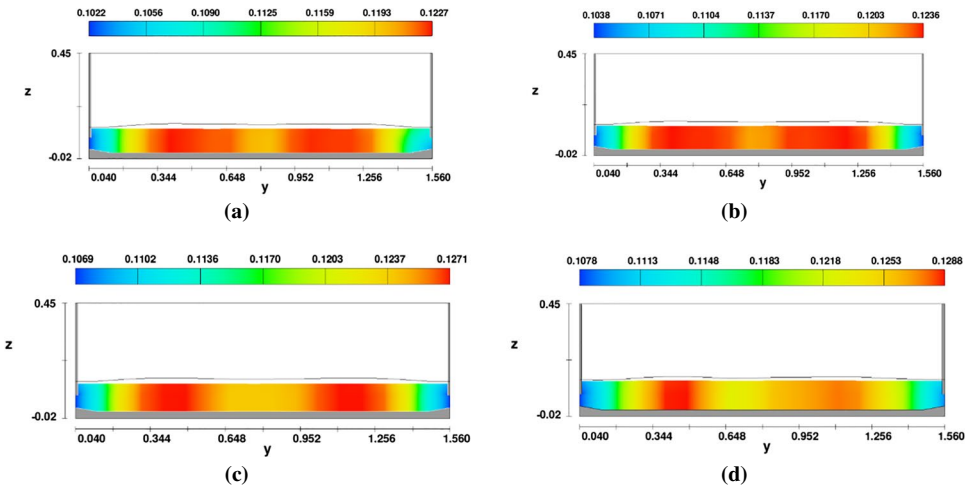

Fig. 8 Flow depth contours in cross-section of a Flow-3D model with a bed slope of 0.001 and a discharge of 0.7 m^3/s for different bed materials: **a** concrete, **b** sand, **c** fine gravel, and **d** coarse gravel ($k_s = 3$, 5, 7, and 10 mm respectively)

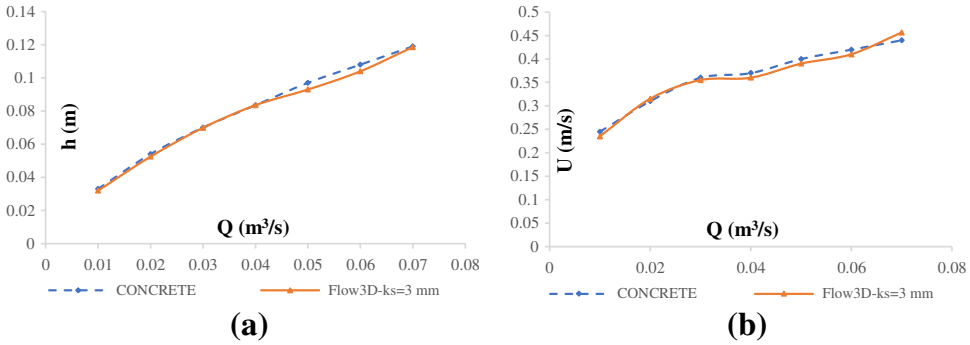

Fig. 9 Verification analysis: **a** stage-discharge curves and **b** average flow velocity; in both numerical and physical models in concrete bed

Table 5 The percentage error of flow depth and average velocity in the numerical model to the physical model

Bed material	Error of depth (%)	Error of averaged velocity (%)
Concrete	2.01	2.64
Sand	2.25	4.23
Fine gravel	2.47	4.84
Coarse gravel	2.28	4.18
Averaged values	**2.25**	**3.97**

Conclusions

In this study, by establishing the physical and numerical models of a wide rectangular channel as a PBS with various sizes of bed materials, comprehensive investigation on stage-discharge and flow resistance of PBSs has been conducted. In the physical model, to investigate the effects of bed material on flow parameters, four different material types have been used. For verifying the numerical model, the flow rate of 0.1 to 0.7 m^3/s and bed slope of 0.001 were applied, and then, the results of the numerical model were compared with the results of the physical model. The FLOW-3D models

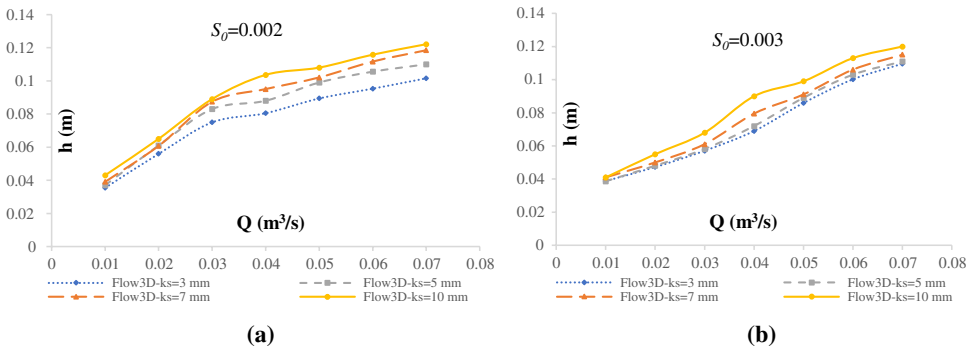

Fig. 10 Stage-discharge curves for PBSNMs with bed slopes of **a** $S_0=0.002$ and **b** $S_0=0.003$

Table 6 Power law stage-discharge relationship for having bed slopes of 0.002 and 0.003 (Eqs. 20–29)

Bed material	*Equation for* $S_0=0.002$	*Equation number*	R^2	*Equation for* $S_0=0.003$	*Equation number*	R^2
Concrete ($k_s=3$ *mm*)	$Q=4.138\times h^{1.83}$	*Equation 20*	*0.978*	$Q=3.355\times h^{1.712}$	*Equation 25*	*0.948*
Sand ($k_s=5$ *mm*)	$Q=2.811\times h^{1.74}$	*Equation 21*	*0.969*	$Q=3.005\times h^{1.684}$	*Equation 26*	*0.957*
Fine gravel ($k_s=7$ *mm*)	$Q=2.358\times h^{1.703}$	*Equation 22*	*0.974*	$Q=3.076\times h^{1.723}$	*Equation 27*	*0.961*
Coarse gravel ($k_s=10$ *mm*)	$Q=2.657\times h^{1.792}$	*Equation 23*	*0.976*	$Q=2.580\times h^{1.750}$	*Equation 28*	*0.985*
Best fit curve	$Q=2.456\times h^{1.698}$	*Equation 24*	*0.9375*	$Q=2.707\times h^{1.668}$	*Equation 29*	*0.9416*

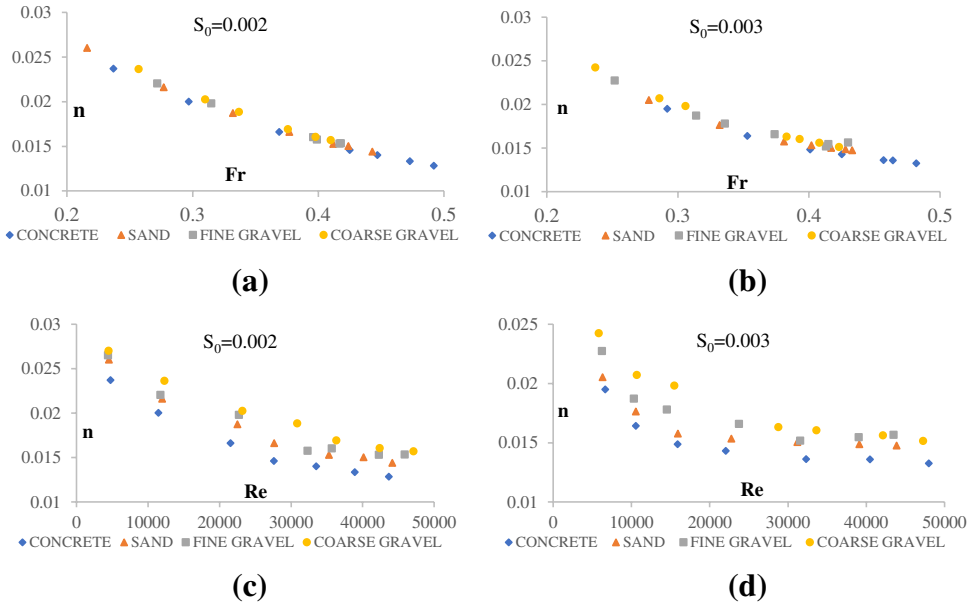

Fig. 11 Variations of n versus **a** *Fr* number for $S_0 = 0.002$, **b** *Fr* number for $S_0 = 0.003$, **c** *Re* number for $S_0 = 0.002$, **d** *Re* number for $S_0 = 0.003$ in Flow-3D models

developed on two PBS models with bed slopes of 0.002 and 0.003. Based on the physical model results, it can be stated that as the flow discharge increased, the Manning's roughness coefficient, *n*, of the flow decreased, and by increasing the *Fr* and *Re* numbers, the Manning's roughness coefficient, *n*, and decreases for all models. Also, the other results show that by increasing R_h/k_s, the Manning's roughness coefficient, *n*, decreases, and by increasing the *b/h* aspect ratio, the Manning roughness coefficient, *n*, increases. Based on the numerical model results, it can be stated that by increasing *Fr* number, the Manning's roughness coefficient, *n*, decreases in both slopes. Results reveal that in the model with $S_0 = 0.002$ for the same values of R_h/k_s, Manning's coefficient, *n*, is higher than that of *n* obtained from the model with $S_0 = 0.003$. Also, concerning the results, it is evident that by increasing the *b/h* aspect ratio, in all bed materials, Manning's roughness coefficient, *n*, increases, and by increasing the R_h/k_s, the effect of *b/h* the aspect ratio on roughness coefficient, *n*, increases. Finally, a new general linear equation for calculating Manning's roughness coefficient, *n*, with all the valid parameters was also obtained that can be used by the hydraulic engineers, and institutional river managers.

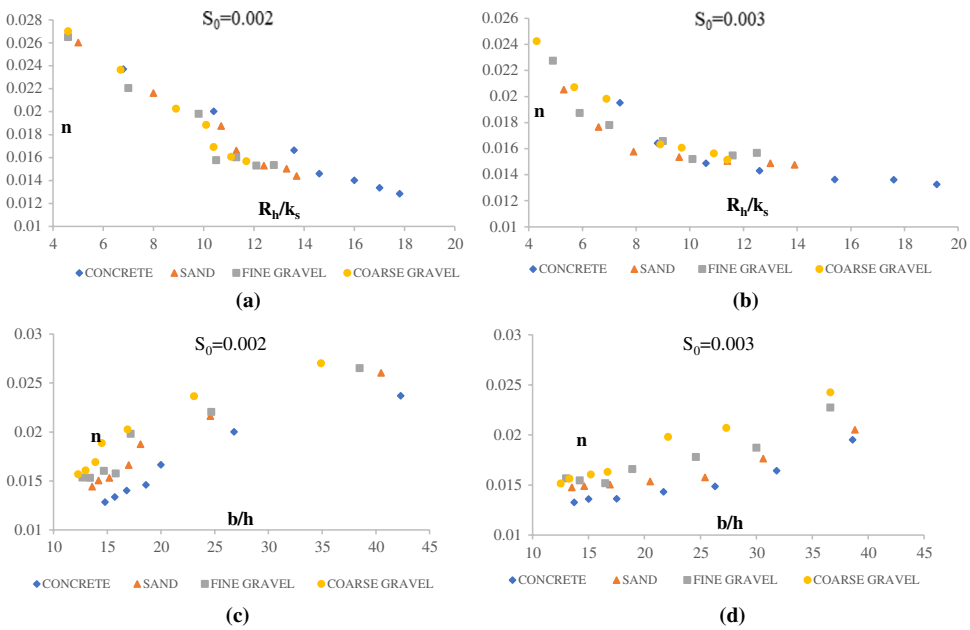

Fig. 12 Variations of *n* versus **a** R_h/k_s for $S_0 = 0.002$, **b** R_h/k_s for $S_0 = 0.003$, **c** *b/h* for $S_0 = 0.002$, **d** *b/h* for $S_0 = 0.003$; by Flow-3D models

Table 7 Equations of the Manning's roughness coefficient, n, and (R_h/k_s) on bed slopes of 0.002 and 0.003 (Eqs. 30–31)

Bed slope (S_0)	Equation	Equation no	R^2
0.002	$n = 0.037 - 0.0025\left(\frac{R_h}{k_s}\right)$	*Equation 30*	*0.964*
0.003	$n = 0.0302 - 0.0021\left(\frac{R_h}{k_s}\right)$	*Equation 31*	*0.905*

Table 8 Specifications of the model used for the overall determination of Manning's roughness coefficient, n

Model	R	R^2	Adjusted R^2	Std. Error of Estimation	Percentage error (%)
1	0.950 [a]	0.902	0.896	0.00099	3.15

[a]Predictors: (constant), Fr, S_0, b/h, R/k_s

Acknowledgements The authors would like to thank Mr. Mahmood Hasanzadeh for providing the field laboratory place. Best thanks to Mr. Ayoub Ghafouri for his technical support.

Declarations

Conflict of interest The authors declare no competing interests.

References

Abril JB, Knight DW (2004) Stage-discharge prediction for rivers in flood applying a depth-averaged model. J Hydraul Res 42(6):616–629. https://doi.org/10.1080/00221686.2004.9628315

Akan AO (2006) Open Channel Hydraulics. Elsevier, London, p 69

Buffington JM, Montgomery DR (1999) Effects of hydraulic roughness on surface textures of gravel-bed rivers. Water Resour Res 35(11):3507–3521. https://doi.org/10.1029/1999WR900138

Buffington JM, Montgomery DR (2013) Geomorphic classification of rivers. In: Shroder J, Wohl E (eds) Treatise on Geomorphology; Fluvial Geomorphology, vol 9. Academic Press, San Diego, pp 730–767. https://doi.org/10.1016/B978-0-12-374739-6.00263-3

Cantalice JRB, Cunha Filho M, Stosic BD, Piscoya VC, Guerra SM, Singh VP (2013) Relationship between bedload and suspended sediment in the sand-bed Exu River, in the semi-arid region of Brazil. Hydrol Sci J 58(8):1789–1802. https://doi.org/10.1061/(ASCE)0733-9429(2008)134:6(847)

Dolgopolova E (2000) The Coefficient of Friction in Channel Flows. J Water Resources 27(6):611–616. https://doi.org/10.1023/A:1026665902849

Dolgopolova E (2001) Plane River Resistance. XXIX IAHR congress-Hydraulics of Rivers, Water Works and Machinery, Beijing, pp 13–20

Einstein HA, Barbarossa NL (1952) River channel roughness. Trans ASCE 117:1121–1146

Ferguson R (2007) Flow resistance equations for gravel- and boulder-bed streams. Water Resour Res. https://doi.org/10.1029/2006WR005422

Ferguson R (2010) Time to abandon the Manning equation? Earth Surf Process Landf 35:1873–1876. https://doi.org/10.1002/esp.2091

Ferguson R (2012) River channel slope, flow resistance and gravel entrainment thresholds. Water Resour Res. https://doi.org/10.1029/2011WR010850

Flow Science Inc. (2008) FLOW-3D User's Manual. 9.3 editions

Guven A, Aytek A (2009) New approach for stage–discharge relationship: gene-expression programming. J Hydrol Eng 14(8):812–820. https://doi.org/10.1061/(ASCE)HE.1943-5584.0000044

Hasanpour Kashani M, Daneshfaraz R, Ghorbani MA, Najafi MR, Kisi O (2015) Comparison of different methods for developing a stage–discharge curve of the Kizilirmak River. J Flood Risk Manag 8(1):71–86. https://doi.org/10.1111/jfr3.12064

Hinze JO (1975) Turbulence, 2nd edn. McGraw-Hill, New York

Horacio J, Ollero A, Pérez-Alberti A (2017) Geomorphic classification of rivers: a new methodology applied in an Atlantic Region (Galicia, NW Iberian Peninsula). Environ Earth Sci 76(21):746. https://doi.org/10.1007/s12665-017-7072-0

Horacio J, Montgomery DR, Ollero A, Ibisate A, Pérez-Alberti A (2018) Application of lithotopo units for automatic classification of rivers: concept, development and validation. Ecol Ind 84:459–469. https://doi.org/10.1016/j.ecolind.2017.08.043

Hou J, Zhang C, Wang D, Li F, Yu Z, Zhou Q (2019) Fixed-bed and mobile-bed resistance of channels with steep gradients in mountainous areas. Water 11(4):681. https://doi.org/10.3390/w11040681

Iraji H, Mohammadi M, Shakouri B, Meshram SG (2020) Predicting reservoir volume reduction using artificial neural network. Arab J Geosci 13(17):1–13

Jain SK, Chalisgaonkar D (2000) Setting up stage-discharge relations using ANN. J Hydrol Eng 5(4):428–433. https://doi.org/10.1061/(ASCE)1084-0699(2000)5:4(428)

Javid S, Mohammadi M (2012) Boundary shear stress in a trapezoidal channel. Int J Eng 25(4):323–331. https://doi.org/10.5829/idosi.ije.2012.25.04a.04

Julien PY (2010) Erosion and sedimentation. Cambridge University Press, Cambridge

Karim F (1999) Bed-form geometry in sand-bed flows. J Hydraul Eng 125(12):1253–1261. https://doi.org/10.1061/(ASCE)0733-9429(1999)125:12(1253)

Kasprak A, Hough-Snee N, Beechie T, Bouwes N, Brierley G, Camp R, ..., Wheaton J (2016) The blurred line between form and process: a comparison of stream channel classification frameworks. PLoS ONE 11(3):e0150293. https://doi.org/10.1371/journal.pone.0150293

Kumar B (2011) Flow resistance in alluvial channel. Water Resour 38(6):745–754. https://doi.org/10.1134/S009780781106008X

Kumar B, Bhatla A (2010) Genetic algorithm optimized neural network prediction of friction factor in a mobile bed channel. J Intell Syst 19(4):315–336 (https://www.degruyter.com/downloadpdf/journals/jisys/19/4/article-p315.xml)

Léonard J, Mietton M, Najib H, Gourbesville P (2000) Rating curve modelling with Manning's equation to manage instability and improve extrapolation. Hydrol Sci J 45(5):739–750. https://doi.org/10.1080/02626660009492374

Leopold LB, Wolman MG, Miller JP (1964) Fluvial processes in geomorphology. Freeman, San Francisco

Lopez R, Barragan J (2008) Equivalent roughness of gravel-bed rivers. J Hydraul Eng 134–6:847–851. https://doi.org/10.1061/(ASCE)0733-9429(2008)134:6(847)

Lotter GK (1933) Considerations on hydraulic design of channels with different roughness of walls, vol 9. Transactions, All-Union Scientific Research Institute of Hydraulic Engineering, Leningrad, pp 238–241

Maghrebi MF (2006) Application of the single point measurement in discharge estimation. Adv Water Resour 29(10):1504–1514. https://doi.org/10.1016/j.advwatres.2005.11.007

Maghrebi MF, Ahmadi A, Attari M, Maghrebi RF (2016) New method for estimation of stage-discharge curves in natural rivers. Flow Meas Instrum 52:67–76. https://doi.org/10.1016/j.flowmeasinst.2016.09.008

Meyer-Peter E, Müller R (1948) Formulas for bed-load transport. In: IAHSR 2nd meeting, Stockholm, appendix 2. IAHR. http://resolver.tudelft.nl/uuid:4fda9b61-be28-4703-ab06-43cdc2a21bd7

Mohammadi M (1998) Resistance to flow and the influence of boundary shear stress on sediment transport in smooth rigid boundary channels. PhD Thesis, Submitted to the School of Civil Eng., The University of Birmingham

Mohammadi M (2002) On the effect of shape on resistance to flow in open channels. Proceedings International Conference on: Fluvial Hydraulics (Riverflow2002), Louvain-La-Neuve, 3–6 September, Belgium: 339–348

Myers WRC (1982) Flow resistance in wide rectangular channels. J Hydraul Div ASCE 108(4):471–482

Nezu I, Rodi W (1986) Open channel flow measurements with a laser doppler anemometer. J Hydraul Eng ASCE 112(5):335–355. https://doi.org/10.1061/(ASCE)0733-9429(1986)112:5(335)

Nitsche M, Rickenmann D, Turowski JM, Badoux A, Kirchner JW (2011) Evaluation of bedload transport predictions using flow resistance equations to account for macro-roughness in steep mountain streams. Water Resour Res. https://doi.org/10.1029/2011WR010645

Parsaie A, Najafian S, Omid MH (2017) Stage discharge prediction in heterogeneous compound open channel roughness. ISH J Hydraul Eng 23(1):49–56. https://doi.org/10.1080/09715010.2016.1235471

Powell MD (2014) Flow resistance in gravel-bed rivers. Progr Res 136:301–338. https://doi.org/10.1016/j.earscirev.2014.06.001

Rahimpour M, Maghrebi MF (2006) Prediction of stage–discharge curves in open-channels using a fixed-point velocity measurement. Flow Meas Instrum 17(5):276–281. https://doi.org/10.1016/j.flowmeasinst.2006.07.001

Raudkivi AJ (1967) Analysis of resistance in fluvial channels. J Hydraul Div 93(HY5):2084–2093

Richardson EV, Simons DB (1967) Resistance to flow in sand channels. In Proceeding of12th IAHR world congresses. Fort Collins, Colorado, U.S.

Rosgen DL (1994) A classification of natural rivers. CATENA 22(3):169–199. https://doi.org/10.1016/0341-8162(94)90001-9

Rosgen DL (2003) Applied River Morphology. University of East Anglia, Norwich, p 27 (**PhD dissertation, plus appendices**)

Rosgen DL, Silvey HL (1996) Applied river morphology, vol 1481. Wildland Hydrology, Pagosa Springs

Rouse H (1965) Critical analysis of open-channel resistance. J Hydraul Div Am Soc Civ Eng (ASCE) 91(HY4):1–25

Roushangar K, Saghebian SM, Mouaze D (2017) Predicting characteristics of dune bedforms using PSO-LSSVM. Int J Sedim Res 32(4):515–526. https://doi.org/10.1016/j.ijsrc.2017.09.005

Satvati S, Alimohammadi H, Rowshanzamir M, Hejazi SM (2020) Bearing capacity of shallow footings reinforced with braid and geogrid adjacent to soil slope. Int J Geosynth Ground Eng 6(4):1–12. https://doi.org/10.1007/s40891-020-00226-x

Schlichting H, Kestin J (1961) Boundary layer theory, vol 121. McGraw-Hill, New York

Sefe FTK (1996) A study of the stage-discharge relationship of the Okavaiigo River at Mohembo, Botswana. Hydrol Sci J 41(1):97–116. https://doi.org/10.1080/02626669609491481

Singh VP, Cui H, Byrd AR (2014) Derivation of rating curve by the Tsallis entropy. J Hydrol 513:342–352. https://doi.org/10.1016/j.jhydrol.2014.03.061

Sivapragasam C, Muttil N (2005) Discharge rating curve extension–a new approach. Water Resour Manag 19(5):505–520. https://doi.org/10.1007/s11269-005-6811-2

Smith KV (1968) Alluvial channel resistance related to bed form. J Hydraul Div 94(1):59–70 (https://cedb.asce.org/CEDBsearch/record.jsp?dockey=0015270)

Sterling M, Knight DW (2000) Resistance and boundary shear in circular conduits with flat beds running part full. Proceedings of the Institution of Civil Engineers-Water and Maritime Engineering, vol 142. Thomas Telford Ltd., London, pp 229–240

Taylor RH Jr, Brooks NH (1962) Discussion of resistance to flow in alluvial channels. Trans Am Soc Civ Eng 127:982–992

Van der Mark CF, Blom A, Hulscher SJMH (2008) Quantification of variability in bedform geometry. J Geophys Res: Earth Surf 113(F3):1. https://doi.org/10.1029/2007JF000940

Van Rijn LC (1984) Sediment transport, part III: bed forms and alluvial roughness. J Hydraul Eng 110(12):1733–1754. https://doi.org/10.1061/(ASCE)0733-9429(1984)110:12(1733)

White W, Paris E, Bettess R (2005) A new general method for prediction of the frictional characteristics of alluvial streams. Wallingford, Report No.187, England.

Yang K, Liu X, Cao S, Huang E (2014) Stage-discharge prediction in compound channels. J Hydraul Eng 140(4):06014001. https://doi.org/10.1061/(ASCE)HY.1943-7900.0000834

Yang SQ, Tan SK, Lim SY (2005) Flow resistance and bed form geometry in a wide alluvial channel. Water resources research, 41(9). https://doi.org/10.1029/2005WR004211

Yang CT (1996) Sediment transport: theory and practice. McGraw-Hill Series in Water Resources and Environmental Engineering.

Yen BC (1991) Channel flow resistance: centennial of Manning's formula. Water Resources Publications, Littleton Colorado, USA, pp 206–222

Yen BC (2002) Open channel flow resistance. Journal of Hydraulic Engineering-ASCE 128(1):20–39. https://doi.org/10.1061/(ASCE)0733-9429(2002)128:1(20)

Yen BC (1992) Hydraulic resistance in open channels. Channel flow resistance-Centennial of Manning's Formula, 1–135.

Zheng J, He H, Alimohammadi H (2021) Three-dimensional Wadell roundness for particle angularity characterization of granular soils. Acta Geotech 16(1):133–149. https://doi.org/10.1007/s11440-020-01004-9